Sedimentary Geology 340 (2016) 15–24

Contents lists available at ScienceDirect

Sedimentary Geology

journal homepage: www.elsevier.com/locate/sedgeo

Coupling of sedimentological and limnological dynamics in subarctic thermokarst ponds in Northern Québec (Canada) on an interannual basis

Olivier Coulombe, Frédéric Bouchard, Reinhard Pienitz *

Centre d'études nordiques (CEN), Université Laval, 2405 de la Terrasse, Québec, QC, G1V 0A6, Canada
Département de Géographie, Université Laval, 2405 de la Terrasse, Québec, QC, G1V 0A6, Canada

ARTICLE INFO

Article history:
Received 22 June 2015
Received in revised form 14 January 2016
Accepted 18 January 2016
Available online 22 January 2016

Keywords:
Sedimentation
Thermokarst ponds
Permafrost
Sediment trap
Subarctic

ABSTRACT

Landscapes are changing at fast rates in subarctic regions due to recent climate warming and related permafrost thaw. As a consequence, thermokarst lakes and ponds are forming and their properties are changing rapidly. Here, we report on the interannual (2012-2014) variability of sedimentological and limnological conditions in a recently formed thermokarst pond in discontinuous permafrost terrain in Northern Quebec, and we discuss various aspects of pond sedimentation processes. Sediment samples from collecting traps and a short core were analyzed for particle size, organic matter content and geochemical composition, as well as ^{14}C dating of a peat sample from the core. Results reveal the preponderance of silts containing 2 to 13% organic matter and an age of 1825–1950 cal. yr. BP for the peat sample. A hypoxic hypolimnion formed in the pond during the short summers. Apparent sedimentation rates (up to 5.5 mm/d) varied in relation to local meteorological conditions and snow cover. The results also reveal major parameters associated with sediment composition, most notably dissolved oxygen in the water column, sampling depth and the year of sampling. Microplankton (20–200 μm) is likely the main source of organic matter, which represents up to 10 to 13% of sediment trap samples, considering its size matching a major grain size mode (44.9–59.0 μm). Using sedimentation rates and an estimation of long-term sediment compaction, the pond's "life span" was calculated at 370 to 600 years. This represents a baseline for the general understanding of the development of young (15–20 years) subarctic thermokarst ponds overlying impermeable soils, and provides an approximate time frame for the potential response of such systems to climate change impacts on northern landscapes.

1. Introduction

Studying past and present climate variations is essential to design and validate reliable climate models which are crucial to the understanding of future climate evolution and its various impacts on the landscape. Some regions are more susceptible to climate change than others, and show fast evolution under changing conditions. It is critical to study these "sentinel" regions where impacts of climate change are more immediate and more readily recognizable. Among these is the Subarctic, a transition zone between the Arctic and temperate regions where landscapes are contrasted depending on latitude and where the transition from discontinuous to continuous permafrost is located. The discontinuous permafrost zone is highly climate-sensitive since temperature and precipitation are among the controlling factors of permafrost stability and thickness (Buteau et al., 2010; Smith et al., 2010). Many studies report increasing ground temperatures and permafrost degradation within this zone over the past 50 years, leading to the northward displacement of the discontinuous-continuous permafrost boundary in eastern Canada (e.g., Beaulieu and Allard, 2003; Vallée and Payette, 2007; Chouinard et al., 2007; Beck et al., 2015) and worldwide (e.g., Romanovsky et al., 2010a, 2010b; Smith et al., 2010, 2012).

In the discontinuous permafrost zone, ice-rich landforms are usually dominated by mounds formed by frost heave when segregated ice lenses grow in the soil (Allard et al., 1996; Calmels et al., 2008b; Fortier et al., 2008; Iwahana et al., 2012). Thawing of ice-rich permafrost leads to ground subsidence and formation of thermokarst ponds and lakes in the depressions (Czudek and Demek, 1970). The development, expansion and drainage of these ponds and lakes are controlled by lateral and vertical permafrost degradation, so they reflect the spatial distribution and depth changes of the permafrost (Chen et al., 2014). Thermokarst aquatic systems also affect the energy balance and thermal dynamics of the surrounding permafrost and can further increase its degradation (Yi et al., 2014). Strong erosive processes associated with permafrost thawing usually create high turbidity in the pond waters,

* Corresponding author at: Département de Géographie et Centre d'études nordiques (CEN), Université Laval, 2405 de la Terrasse, Québec, QC, G1V 0A6, Canada. Tel.: +1 418 656 2131 ext. 7006; fax: +1 418 656 2978.
E-mail address: Reinhard.Pienitz@cen.ulaval.ca (R. Pienitz).

http://dx.doi.org/10.1016/j.sedgeo.2016.01.012
0037-0738/

associated with high sedimentary charges (Jolivel and Allard, 2013). With the recent accelerated permafrost degradation in the discontinuous zone due to climate change (Vallée and Payette, 2007; Jones et al., 2011), the number and size of thermokarst lakes increase rapidly, especially in poorly drained soils such as clays and peatlands (Jolivel and Allard, 2013; Bouchard et al., 2014), although it decreases in some regions, mainly due to drainage (Smith et al., 2005; Jones and Arp, 2015). This results in widespread release of mineral and organic sediments, formerly trapped in permafrost, into aquatic systems (Jolivel and Allard, 2013; Hugelius et al., 2014). Organic matter (OM) that is present in both particulate and dissolved form in thermokarst ponds is involved in the biogeochemical production and emission of methane (CH_4) and carbon dioxide (CO_2) into the atmosphere (Phelps et al., 1998; Walter et al., 2006; Schuur et al., 2009; Laurion et al., 2010). These greenhouse gas (GHG) emissions from thermokarst lakes and ponds thus have the potential to contribute to known positive feedback mechanisms thereby enhancing climate warming (Walter et al., 2006; Schuur et al., 2008; Laurion et al., 2010). Aquatic thermokarst systems have a high impact potential on global climate because of their extended distribution among permafrost regions; Holocene thermokarst basins have been assessed to be a major organic carbon reservoir and thus a potential carbon source upon permafrost thaw (Walter Anthony et al., 2014). Actual thermokarst basins potentially have an equally important impact on modern carbon pool, and an improved understanding of the sedimentary dynamics of these systems is needed.

The aim of this study was to determine the variability of sedimentological and limnological conditions of a thermokarst pond in Northern Québec (Nunavik, Canada) throughout a year, and between different years. An appropriate way to study modern sedimentary processes and dynamics in thermokarst lakes and ponds is the use of sediment traps. This approach has only recently been used in thermokarst ponds (Bouchard et al., 2014) and this study further develops its application. It is part of the broader research program ADAPT (Arctic Development and Adaptation to Permafrost in Transition), aimed at assessing various aspects of permafrost degradation at northern latitudes. More specific objectives of the study were to determine the amplitude and dynamics of sedimentation processes in the pond, and to characterize the relationships between sediment properties, its limnological parameters, and meteorological conditions. Furthermore, the study aimed at identifying patterns that could provide a more generalized understanding of thermokarst pond sedimentological dynamics and a first estimation of their "life span".

2. Study area

2.1. Geological setting, climate and vegetation

The study was conducted in subarctic Québec, on the eastern shore of Hudson Bay, in Nunavik, Canada (Fig. 1). The transition from isolated (< 10% of land surface) to sporadic permafrost (< 50%) and then from discontinuous (> 50%) to continuous (> 90%) permafrost stretches along a south–north gradient/transect between 55° and 58°N. Two sub-zones related to the presence of postglacial Tyrrell Sea deposits (see below) can also be distinguished: plateaus and mounds (lithalsas) in clayey silts (B^1), and palsas overlying fine postglacial sediments (C^1) (Bhiry et al., 2011) (Fig. 1).

Nunavik bedrock is mainly composed of Precambrian granito-gneissic rocks belonging to the Superior geological province (Thériault and Beauséjour, 2012). The Wisconsin glaciation ended around 8000 cal yr. BP in the Hudson Bay region (Hillaire-Marcel, 1976; Dyke and Prest, 1987) and following glacial retreat, the postglacial Tyrrell Sea submerged the landscape up to an elevation of between 244 and 315 m above present-day sea-level (a.s.l.) (Hillaire-Marcel and Fairbridge, 1978; Allard and Séguin, 1985). Due to rapid postglacial isostatic rebound, the sea has receded near its present-day level around 6000 cal yr. BP (Bhiry et al., 2011; Lavoie et al., 2012). Along the present-day coastline of Hudson Bay, permafrost has therefore developed postglacially in marine sediments of the Tyrrell Sea and peatlands (Hillaire-Marcel, 1976; Allard and Seguin, 1987; Bhiry et al., 2011; Lamarre et al., 2012).

In the sporadic and discontinuous permafrost zones, numerous palsas and lithalsas have formed, mostly at the beginning of the so-called Neoglacial cool episode about 3000 years ago and the onset of the Little Ice Age (LIA) (Beaulieu and Allard, 2003; Vallée and Payette, 2007; Bhiry et al., 2011). Permafrost degradation following the LIA led to widespread thawing and the formation of thermokarst ponds during

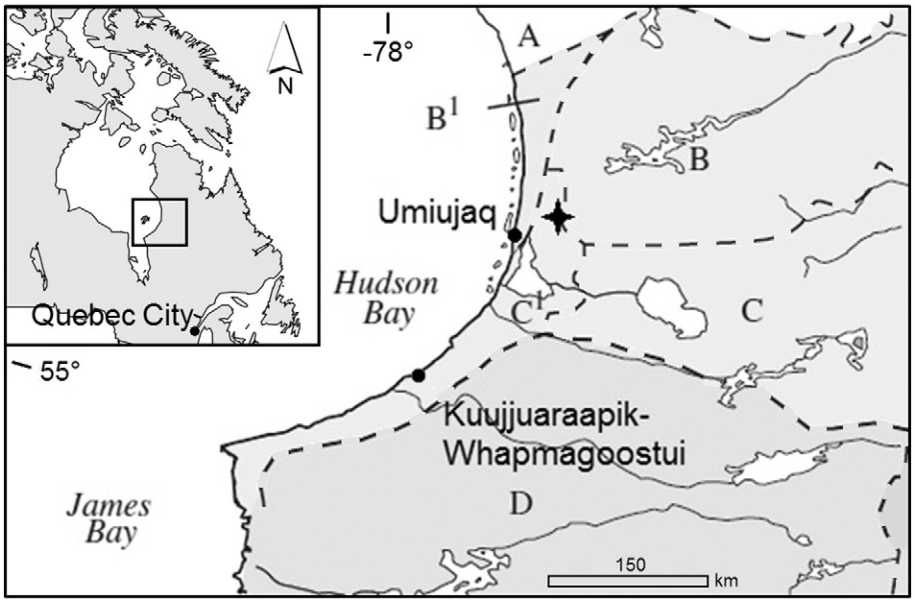

Fig. 1. Study site location (star) and permafrost distribution in subarctic Quebec. (A): Continuous permafrost (> 90% of land surface). (B): Discontinuous permafrost (50–90% of land surface). Sub-zone **B^1**: Major concentration of permafrost area plateaus and mounds in clayey silts of Tyrrell Sea. (C): Sporadic permafrost (10–50% of land surface). Sub-zone **C^1**: Area characterized by palsas overlying fine Tyrrell Sea sediments. (D): Isolated permafrost (< 10% of land surface). Modified from Bhiry et al., 2011.

the past century, particularly during the last decades (Vallée and Payette, 2007; Bhiry et al., 2011; Bouchard et al., 2011).

The meteorological station closest to the study site (active since 1980) is at Kuujjuaraapik-Whapmagoostui, about 150 km SSW of the site, where the mean annual air temperature was −4.0 °C for the period 1981–2010 (Environment Canada, 2015). The coldest month was January, with an average temperature of −23.3 °C, and the warmest August, with an average temperature of 11.8 °C. The average of total annual precipitation was 660.8 mm for the same period, of which 36% fell as snow. A meteorological station from the Centre for Northern Studies (CEN) was active near the study site during the two years of sampling (temperature only). The average temperature recorded from 1 September 2012 to 31 August 2014 was −3.4 °C.

The study area includes, from south to north, the three vegetation types of boreal forest, forest-tundra and shrub tundra. The northern treeline crosses the area near the study site. In addition to temperature and snow cover, vegetation density influences the distribution of permafrost through its thermal effect (Allard and Seguin, 1987). Continuous permafrost matches shrub tundra, while discontinuous permafrost corresponds to forest-tundra cover. Over the last decades, permafrost in marine silts was twice as thick and three times more widespread in shrub tundra than in forest-tundra areas (Allard and Seguin, 1987).

2.2. Study site

The BGR study site (56°36.624 N; 76°12.858 W) is located at 185 m a.s.l. near the transition between the two sub-zones B^1 and C^1, approximately 20 km east-north-east of the Inuit village of Umiujaq (Fig. 1). This area includes numerous small thermokarst ponds (Fig. 2). The majority of these ponds is isolated from the river and has very turbid waters that give them an opaque and milky appearance. The site is also near the boundary between sporadic and discontinuous permafrost, more precisely in the area characterized mainly by lithalsas and a few palsas overlying fine sediments deposited by post-glacial Tyrrell Sea. The soils are essentially mineral, composed mainly of silty clays from the Tyrrell Sea (Calmels et al., 2008a, 2008b). The permafrost at the site and in the vicinity has been reported to be in decay during the last five decades (Allard and Seguin, 1987; Thibault and Payette, 2009; Jolivel and Allard, 2013), and thermokarst ponds have been forming following the melting of the lithalsa ice cores. Of the permafrost that existed in 1957 within the Sheldrake River watershed, 21% is estimated

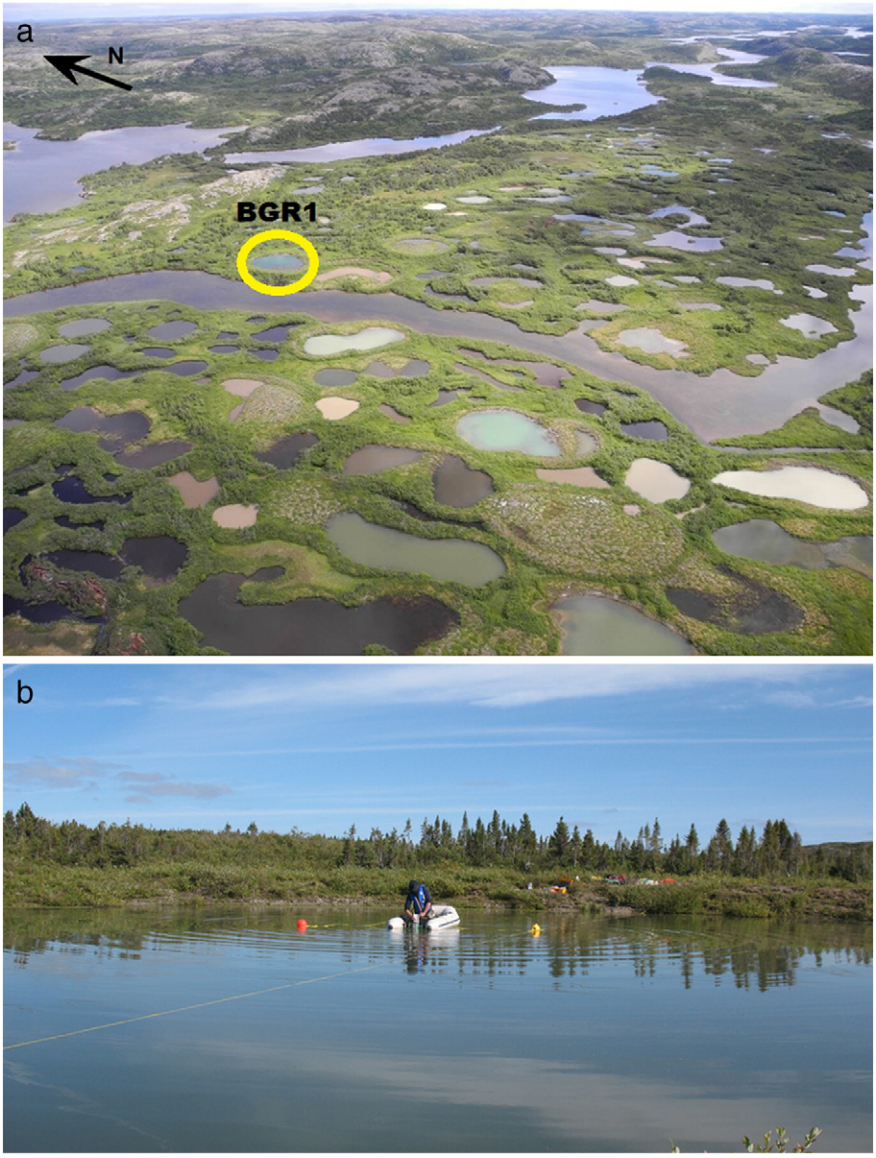

Fig. 2. (a) Oblique aerial photograph taken from a helicopter with identification of the BGR1 pond. The Sheldrake River is visible in the background. (b) Close-up view of the BGR1 pond.

to have disappeared by 2009, and a 96% increase in thermokarst pond coverage has been observed since this time (Jolivel and Allard, 2013).

The pond investigated in this study, unofficially named BGR1, is shown in Fig. 2. It has a nearly circular shape (length = 41 m, width = 30 m) and its maximum depth is ~4.3 m. It is surrounded by a 1–2 m high peripheral ridge delimiting the former border (contours) of a thawed lithalsa (Calmels et al., 2008a). There are some uncertainties regarding possible water level fluctuations, as the maximum depth measured was different each summer (3.4 m in 2012, 4.3 m in 2014). Slopes are rather steep (25%) (Proult, 2014) and catchment size is almost equivalent to the surface area of the pond, i.e., within the limits of the peripheral ridge. The pond appeared less than 50 years ago, most likely 15–20 years ago, and reached its current extent less than ten years ago, as evidenced by aerial photographs presented in Calmels et al. (2008a).

3. Materials and methods

3.1. Field sampling

The first step was to sample sediments within the pond on a yearly basis using sediment traps. This type of device has been widely used in lakes by the scientific community since 1900 (Gardner, 1980b). Numerous studies have assessed this method through both laboratory and field-based approaches in standing waters (Kirchner, 1975; Hargrave and Burns, 1979; Gardner, 1980a, 1980b; Baker et al., 1988; Köster and Pienitz, 2006) and many designs have been developed to be site-specific (Gardner, 1977, 1980a; Honjo and Doherty, 1988).

In summer 2012, an optical sediment trap was installed at the bottom of pond BGR1 with two adjacent simple traps (Fig. 3). In summer 2013, the latter were removed and transported to the laboratory and replaced by two new simple traps, this time installed at different depths. One was placed near the bottom of the pond in the oxygen-poor hypolimnion and the other 1 m above it, where the water column is richer in oxygen. A short (< 20-cm long) sediment core was also retrieved near the shore (~ 0.5 m water depth) and subsampled at three different depths: at the surface (0–2 cm) in silt-clay; at 13–14 cm, also in silt-clay; and at 15–16 cm in peat. In summer 2014, material gathered by the traps installed during the preceding year was retrieved, and surface sediment (0–2 cm) from the bottom of the pond was also sampled. During the summers of 2012 and 2014, limnological profiles of temperature, specific conductivity, dissolved oxygen (DO) and pH were measured at every ~50 cm throughout the water column using a multiparameter water quality sonde (YSI EXO). A 20 cm-diameter Secchi disk was used to determine water transparency, whereas total suspended solid (TSS) concentrations in surface waters were measured using precombusted and preweighed glass fiber filters (0.7 mm nominal mesh size; Advantec MFS Inc., Dublin, California) that were subsequently dried for 24 h at 60 °C. Dissolved organic carbon (DOC) concentrations were measured using a Shimadzu TOC-500 A carbon analyzer calibrated with potassium biphthalate in samples filtered through prerinsed cellulose acetate filters (0.2 mm pore size; Advantec

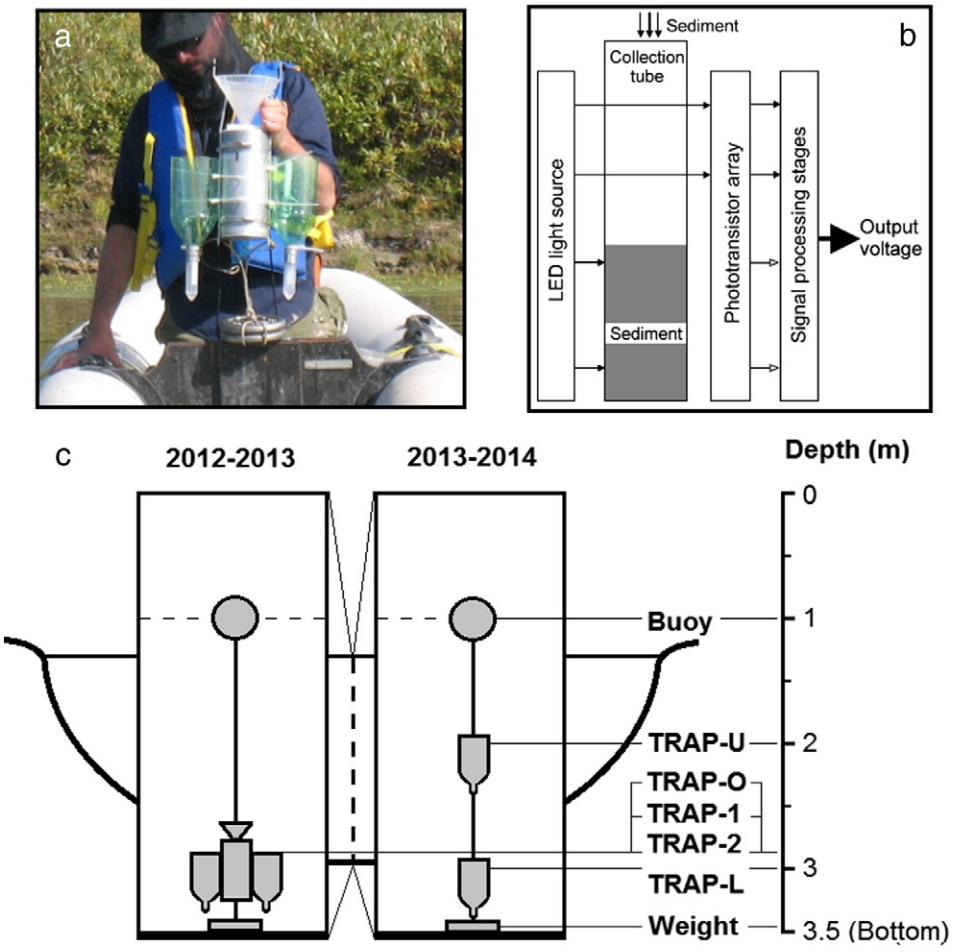

Fig. 3. (a) Photograph of the sediment trap set-up just before its installation in the pond in August 2012. (b) Diagram showing the main functional components of the optical sediment trap (modified from Lamoureux, 2005). (c) Diagram presenting a profile of the BGR1 pond and the sediment trap set-up for years 2012–2013 and 2013–2014. See Table 1 for sample description.

MFS Inc.). All samples were kept in prewashed Teflon-capped glass bottles and preserved at 4 °C until analysis.

The sediment trap used during the years 2012 and 2013 consists of an optical system and a data-logger made by Onset Computer Corporation (model "Hobo Temperature, ext. (C) 1996") assembled in a submersible housing as presented in Lamoureux (2005). This battery-powered device steadily records, on a 6-h interval, temperature and light transmission, which is controlled by the accumulation of sediments within a transparent tube (Fig. 3b). Columns of light sources and light sensors are installed at opposite sides of the tube such that sediments eventually prevent sensors from receiving the light. A circuit converts signals from the sensors in an output voltage, which is in linear relation to the sediment blockage (Lamoureux, 2005). Taking into account the amplification ratio (16:1) from the use of a funnel to enhance the quantity of sediment collected, the measured voltage can be transformed into apparent sediment thickness values, from which accumulation rates can be inferred. Other sediment traps used in association with the optical trap between 2012 and 2013 and at different depths between 2013 and 2014 are simple plastic funnels (10.2 cm diameter) with 50-ml plastic tubes as receptacles.

Traps were mounted on a rope with a weight at one end to stay anchored at the bottom of the pond, and a buoy at the other end to tighten the rope vertically. The buoy was placed at an approximate depth of 1 m below the water surface, in order to avoid any interaction with winter ice cover. In summer 2012, the optical trap combined with the two simple traps was installed 60 cm above the weight at the bottom of the pond (3.5 m depth) (Fig. 3c). In summer 2013, two simple traps were placed at approximate depths of 2 m and 3 m, for the purpose of observing the effects of changing water column properties (e.g., DO) on sediment material accumulation.

3.2. Laboratory analyses

A total of 9 sediment samples was transported from the field to the Aquatic Paleoecology Laboratory of Centre for Northern Studies (CEN) at Laval University where they were freeze-dried (24 to 48 h) or oven-dried (50 °C) until completely dry. Table 1 shows the sample codes, their composition, origin and year of sampling.

Two replicates of a peat sample from below the mineral sediments (15–16 cm core depth) were ^{14}C AMS dated. The analysis was conducted at Keck Carbon Laboratory of the University of California Irvine, in collaboration with the Radiochronology Laboratory of CEN. Results obtained in ^{14}C years BP were calibrated to calendar years BP with the CALIB 7.0.2 program (Stuiver et al., 2005).

Particle-size analysis was conducted on all other core and trap samples to study sediment variability relative to depth and year and to provide insights on the pond major sediment sources. Ultrasonic treatment was used to deflocculate clay-sized particles just before using a laser diffraction analyzer (Model Partica LA95-v2 from Horiba), following the protocol from Cayer (2010).

Table 1
Names and types of samples, their origin and year of sampling. See Fig. 3c for a spatio-temporal representation of trap samples.

Sample name	Material	Origin	Year
TRAP-O	Silt/Clay	Optical trap	2012–2013
TRAP-1	Silt/Clay	Simple trap	2012–2013
TRAP-2	Silt/Clay	Simple trap	2012–2013
CORE-S13	Silt/Clay	Bottom of pond (Core surface)	2013
CORE-DEEP	Silt/Clay	Core 13–14 cm	2013
CORE-PEAT	Peat	Core 15–16 cm	2013
TRAP-U	Silt/Clay	Upper (2 m depth) simple trap	2013–2014
TRAP-L	Silt/Clay	Lower (3 m depth) simple trap	2013–2014
CORE-S14	Silt/Clay	Bottom of pond	2014

To estimate OM content in the samples, loss-on-ignition (LOI) analyses were conducted following the method of Heiri et al. (2001). Samples of approximately 1 g were weighed, then placed in the oven at 550 °C for four hours, then weighed again to obtain weight loss in the process, which generally corresponds to OM content. The proportions of carbon (C), hydrogen (H) and nitrogen (N) in the samples were also measured at CEN's Radiochronology Laboratory using a LECO CHN628 Elemental Analyzer.

3.3. Pond "life span" estimation

Calculations of the time required for the total infilling of the BGR1 pond were based on a compaction coefficient (CC), which was determined using particle density (d) of the sediments collected in the pond. Particle density was calculated using standardized values for mineral sediments and organic matter: 2.65 g/cm^3 for the mineral fraction and 1.25 g/cm^3 for the organic fraction (Boyd, 1995). CC is the ratio between dry sediment (buried) volume and wet sediment (newly settled) volume:

$$CC = \frac{Dry\ sediment\ mass\ (g)/d}{Water\ content\ (cm^3) + (Dry\ sediment\ mass\ (g)/d)} \quad (1)$$

The time (T) required for the infilling of the pond with compacted sediments can then be calculated using the raw sediment input per year in the pond and the depth of the pond:

$$T = \frac{Depth\ (m)}{Yearly\ sediment\ input\ (m/y) \times CC} \quad (2)$$

4. Results

4.1. Limnology

The average Secchi depths were 1.15 m and 2 m, measured in August 2012 and 2014 respectively. These values are higher than those recorded in most of the thermokarst ponds in the region (e.g., Bouchard et al., 2014), meaning clearer waters. TSS and DOC in surface water were 2.4 mg/L and 3.5 mg/L, respectively, in August 2012. In July 2013, DOC varied between 2.7 mg/L at the bottom, 2.7 mg/L at the center surface of the pond, and 3.0 mg/L at the surface near the shore. Fig. 4

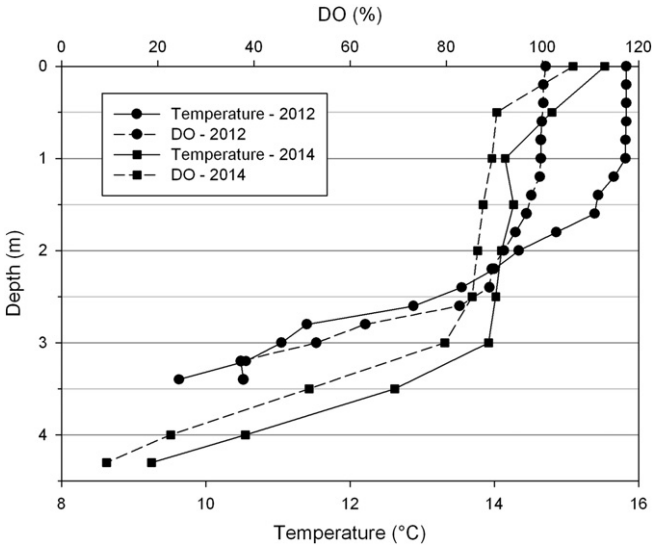

Fig. 4. Temperature and dissolved oxygen (DO) profiles relative to depth as measured on 9 August 2012 and 28 August 2014.

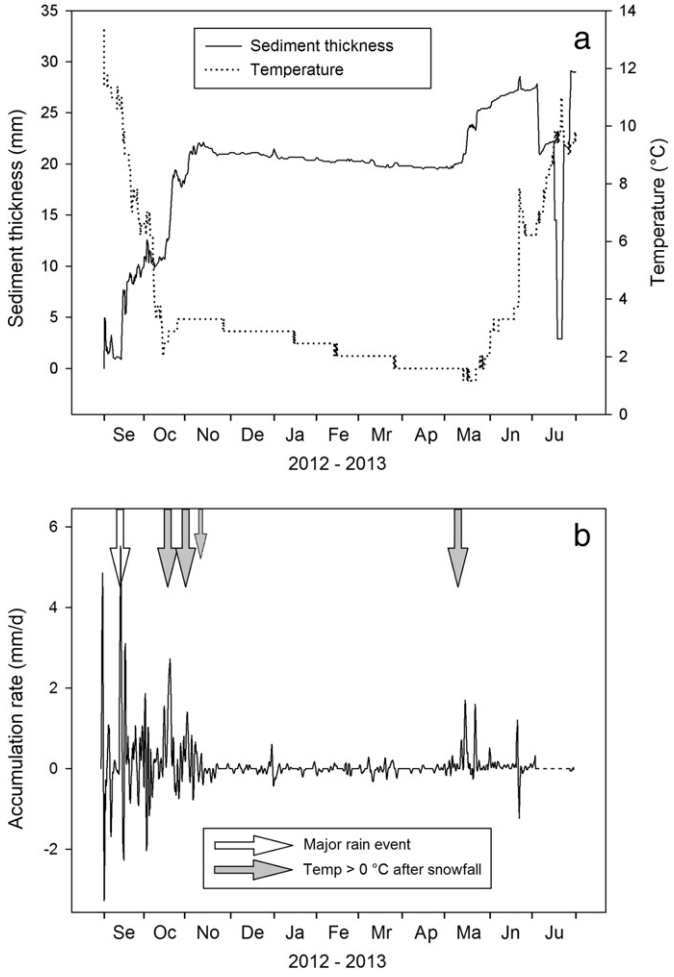

Fig. 5. (a) Apparent sediment thickness, water temperature and (b) accumulation rate measured by the optical trap between 31 August 2012 and 31 July 2013.

shows the temperature and DO profiles relative to depth as measured on 9 August 2012 and 28 August 2014. It reveals temperature and DO decreasing with depth, and thus water column stratification despite a rather shallow depth. In 2012, when analytical resolution was best, temperatures started to decrease at 1 m and then decreased drastically below 1.6 m. DO started to decrease at 1.2 m and dropped abruptly at 2.4 m. A seasonal hypolimnion with a colder, dense bottom water layer can be identified, with its upper limit at about 2 m depth during summer. DO was about 92% at 2 m and only 53% at 3 m in August 2012.

4.2. Optical trap

The optical trap continuously recorded temperature and apparent sediment thickness from its water immersion on 31 August 2012 until it was retrieved on 31 July 2013 (Fig. 5). Sediment thickness quickly increased to more than 20 mm between early September and early November. It then slowly and steadily decreased to below 20 mm until mid-May, when it abruptly increased to nearly 28 mm at the end of June. Data from July 2013 seem erroneous as it drops straight down and then rises again. Temperature dropped from about 13 °C in early September to 2 °C in mid-October. It then slowly decreased until mid-May, to reach a minimum of 1.2 °C, and then quickly increased to 10 °C in July.

The highest apparent sedimentation rates (up to 5.5 mm/d) occurred in September (July excluded) before they slowly decreased until 9 November 2012, after which they became very low. Another high sedimentation period occurred in May 2013 (up to 1.7 mm/d). The month of June was characterised by lower sedimentation rates between spring and late summer maxima (generally under 0.2 mm/d).

The sediment sampling over two consecutive years allowed us to perform a year-to-year variability analysis. Variables that can be compared are the particle size, the organic matter content and the C, H and N composition. Taking into account changes in DO and other pond limnological conditions, the above-mentioned variables can be compared and summarized:

- OM content as well as C% and H% was higher in 2013–2014 than in 2012–2013. The proportions are similar between the years but the values (%) are higher in 2013–2014.
- Particle size decreased from 2012 to 2013 to 2013–2014, from coarse silt to fine silt in samples from the sediment traps.

4.3. Organic matter (OM) and C, H, N composition

Silt samples contained between 2 and 13% of OM, whereas the peat samples contained >80% (Table 2). Material collected by traps contained significantly higher OM proportions (> 10%) than other silt samples (< 6.3%). The highest values were recorded in TRAP-U with 12.5% and the lowest in CORE-S14 with 2.3%. The percentage of C in the samples was correlated to LOI, as shown in Table 2. The percentages of H and N followed the same general trend, except for a few deviations. Trap samples contained 4–5% C, 0.9–1.0% H and 0.4–0.6% N. Other silt samples contained 0.9–2.6% C, 0.3–0.6% H, and more or less 0.1% N.

4.4. Particle size analysis

Most of the samples, namely CORE-DEEP, TRAP-O, TRAP-1, TRAP-2, TRAP-U and TRAP-L were bimodal, with a fine silt mode between 10.1 and 15.2 μm and a coarse silt mode between 44.9 and 59.0 μm depending on the sample (Fig. 6). Fine silts were more important in TRAP-U, TRAP-L and CORE-DEEP, while coarse silts were more important in TRAP-O, TRAP-1 and TRAP-2. CORE-S13 and CORE-S14 only contained fine silts with respective mean grain size values of 8.9 and 10.1 μm.

All samples with coarse silt as the main mode (TRAP-O, TRAP-1 and TRAP-2) were collected in 2012–2013, whereas samples in which fine silts predominated (TRAP-L, TRAP-U) were collected in 2013–2014. The CORE-DEEP sample is also bimodal and its main mode consists of fine silt. This sample has been taken at a depth of 14–15 cm from the core, just above the peat sample, so it is much older than the trap samples. The two samples including a single mode (CORE-S13 and CORE-S14) had the finest general particle size and are both recent sediments collected from the bottom of the pond.

Table 2
Percentages of LOI, C, H and N in all samples, arranged from highest to lowest LOI.

Sample name	LOI (%)	C %	H %	N %
CORE-PEAT	80.40	46.37	5.78	2.32
TRAP-U	12.51	5.10	0.98	0.60
TRAP-L	11.93	4.49	0.95	0.48
TRAP-O	11.07	4.33	0.85	0.55
TRAP-2	10.41	4.03	0.89	0.46
TRAP-1	10.37	4.03	0.91	0.44
CORE-DEEP	6.29	2.64	0.57	0.14
CORE-S13	2.98	0.99	0.37	0.09
CORE-S14	2.26	0.85	0.32	0.06

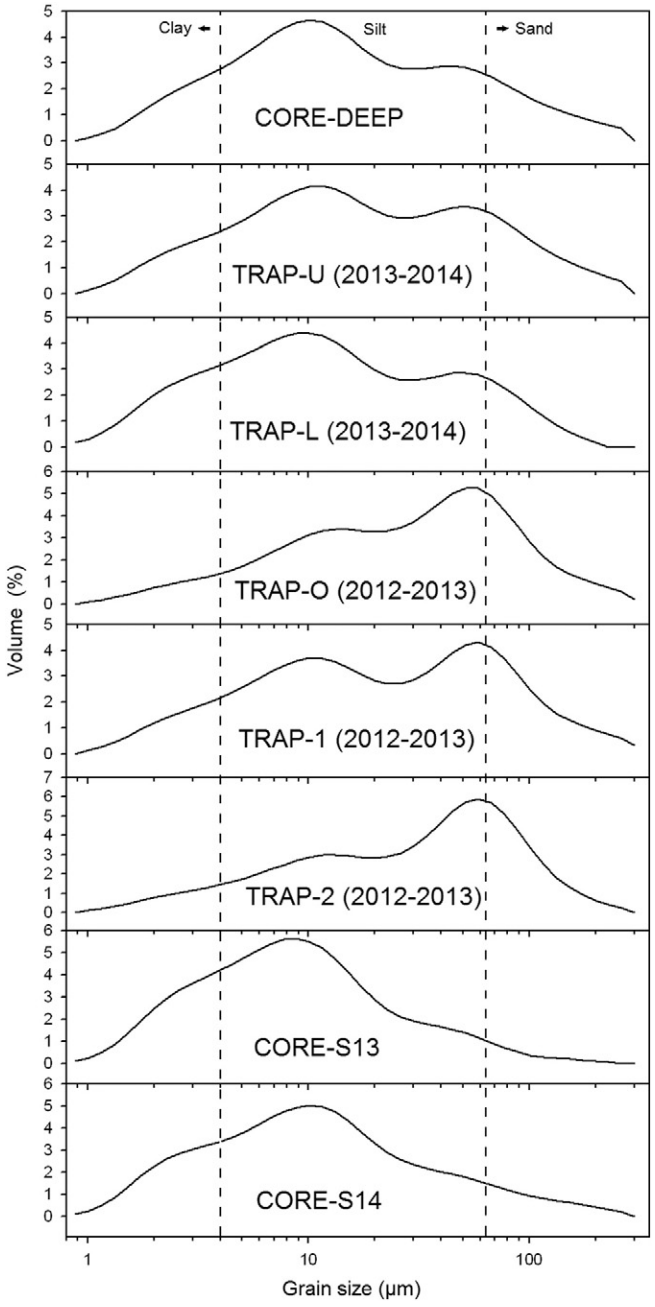

Fig. 6. Grain size distribution of sediments from the samples.

4.5. Peat dating

The peat sample from 15 to 16 cm depth in the short core was dated at 1940 ± 20 ^{14}C yr. BP using two replicates. Age calibration resulted in a range of 1825–1950 cal yr. BP (1σ range).

5. Discussion

5.1. Meteorological forcing on sedimentation rates

Despite the overall positive particle accumulation, sedimentation showed high-amplitude peaks alternating with slightly less pronounced minima (Fig. 5). The absolute values were proportional to the intensity of sedimentation, the most likely explanation being that negative values of accumulation rate corresponded to sediment compaction in the tube. When settling particles enter the tube, the water quickly becomes opaque enough to block light before sediments slowly decant and accumulate to block the light at the level corresponding to their thickness. The positive accumulation rates were therefore over-represented; however, the mean value including both positive and negative rates is representative of sediment accumulation thickness for a given period. Yet, this has to be considered as a preliminary thickness because compaction happens over longer time scales, as indicated during the period from mid-November to early May when thicknesses slowly decreased from 22 to 19.5 mm due to the formation of ice cover that prevented sedimentation (Fig. 5). Such a progressively decreasing trend during winter, though even slower and less pronounced, was observed using an optical sediment trap in a comparable thermokarst pond in southeastern Hudson Bay (Bouchard et al., 2014).

Freezing temperatures and the formation of pond ice and snow cover, which caused the cessation of most erosional processes, likely explain sedimentation interruption during the winter months. On May 15th, 2013, sedimentation resumed due to spring erosional processes associated with snowmelt and water runoff. In a subarctic thermokarst pond like BGR1, sedimentation mainly originates from erosional processes associated with permafrost thaw in the catchment, yet some time is required during the short summers for the ground to warm sufficiently for these processes to be fully activated and for the external sediment inputs to reach their maximum. This explains why sedimentation rates were maximal in September, considering that no data were available for a portion of July and August (Fig. 5). Sediment trap data from nearby thermokarst ponds showed that maximal sedimentation rates were reached earlier in the season, i.e., in July–August (Bouchard et al., 2014). The more southerly location of these ponds, resulting in deeper active layer thawing more rapidly in spring, as well as their smaller size, likely account for this slight difference.

Some major sedimentation events can be associated with the meteorological data. The most important one occurred on September 13th, 2012, when sediment thickness increased from about 1 mm to around 7 mm within only six hours. Several rain showers have been recorded on the preceding day (September 12th) and during the morning of September 13th. This sudden precipitation event probably resulted in erosion and sediment transport in the pond catchment and caused the observed maxima. The next important peak occurred between October 14th and 19th, when sediment thickness rose from 11 to 18.5 mm. No major precipitation events have been directly registered during this time interval, but it corresponds to snowfall from October 11th to October 13th in conjunction with temperatures ≥0 °C. The snow most likely melted and led to runoff, causing the observed peak in sedimentation. The last important sedimentation increase before winter occurred between October 27th and 30th, when thickness increased from 18 to 21 mm. Snow fell on October 23th, 27th and 30th, and rain on October 26th and 29th. Air temperatures remained above 0 °C between October 27th and 30th, leading to a similar signal as compared to previous sedimentation peaks. Such sedimentation peaks following heavy rain or rapidly melted snow precipitations were also reported in similar thermokarst systems of subarctic Québec (Bouchard et al., 2014).

Following the winter months without sedimentation, a first peak occurred on May 15th when temperatures had exceeded 0 °C for 4 days, yet remained below 5 °C and decreased below the freezing point at night. However, as of 9 am on May 14th, temperatures remained above 0 °C all day long and during the following night, reaching a maximum of 10.2 °C at 4 pm on May 15th. This warm spell was likely sufficient to cause the break-up of the pond's ice cover and to initiate sedimentation in the water column, driven by snowmelt, runoff and reactivated pond water circulation.

5.2. Lithalsa development

The presence of peat underneath the silt layer in the BGR1 pond sediment core was rather unexpected as the site is mostly underlain

by mineral soils. Its occurrence could be due to an isolated peat block that collapsed after the thawing of an old palsa, or was part of an extended soil layer. Macro- and microscopic peat debris were indeed found below lacustrine layers of thermokarst ponds south of the BGR site, in a former palsa peatland now in an advanced state of degradation (Bouchard et al., 2011).

Following the marine invasion after the last deglaciation, glacio-isostatic uplift led to a progressive water level decrease in the Sheldrake River watershed, which drains into Hudson Bay (Hillaire-Marcel and Fairbridge, 1978). Near the present-day riverbed including the adjacent BGR site, the landscape was most likely transformed into alluvial plains and then wetlands, which are aquatic ecosystems suitable for peat development. Allard and Seguin (1987) analyzed three permafrost sites including buried peat beds in the forest-tundra zone south of the treeline, in close proximity to the BGR study site. They suggested that climatic conditions were cold enough since land emergence about 5800 years ago to allow for discontinuous permafrost presence, and argued that peat accumulation over unfrozen ground persisted until 2300 to 1400 BP, depending on sites. This timing coincides with the dates obtained on the peat samples (see Section 4.5), which ranged between 1825 and 1950 cal yr. BP. A subsequent burial of the peat layer with silt might be the result of erosion and sediment inputs from surrounding permafrost mounds. Such erosional processes were interpreted by Allard and Seguin (1987) for their study sites. This episode could explain the 14–15 cm thick silt layer overlying the peat in our core from BGR1, including the CORE-DEEP sample. We therefore conclude that the lithalsa responsible for the origin of pond BGR1, despite being mineral, most likely initially developed over peat from ~1825–1950 cal yr. BP at the earliest. The lithalsa was still frozen in 1957, as visible from aerial photographs (Calmels et al., 2008a).

5.3. Sediment properties and limnological parameters interrelation

All analyzed samples generally have a small particle size, being silts or clayey silts. Small particle size usually represents a low-energy environment, as particle size is proportional to the energy required to transport it. However, in environments like the BGR site with erosive processes associated mainly to permafrost thaw, ponds directly receive the material from its source which, in this case, constitutes the permafrost. Hence, the particle size does not really represent the environment's dynamics. Therefore, the high annual sediment charge collected by sediment traps (29 mm total measured by the optical trap) in the BGR1 pond is rather a better indicator of erosional energies associated with permafrost thaw, which seem to be fairly high.

The most important of the two particle size modes recorded in trap samples (the fine silt or the coarse silt mode) appears to be mainly influenced by the year of sampling,that is the different parameters of the environment such as local climatic and hydrological conditions during the year. The most important ones are the different strength of runoff, erosion and biological productivity.

The two finest-grained samples (CORE-S13 and CORE-S14) excluded the coarser gain size mode. They were both recent sediments collected from the bottom of the pond (though not at the same water depth) and yielded the lowest LOI values. This could indicate that the coarse silt mode is possibly associated with and composed of organic particles. The mode (44.9–59.0 μm) corresponds to microplankton (20–200 μm), which should be taken into consideration as the major OM component in the pond constituting sediment samples. Calculated C/N ratios of all samples containing recent sediments (CORE-DEEP and CORE-PEAT excluded) are low (< 15), which supports a mainly autochthonous (lacustrine algae) origin for sedimentary organic matter (Meyers and Teranes, 2001). However, sediment trap samples only have 10 to 13% OM, so that the minerogenic fraction contributes to a much greater extent to the grain size spectrum. Therefore, the mode is likely not entirely composed of microplankton. The CORE-S14 sample represents the upper 0–2 cm of sediments at the pond bottom in summer 2014, whereas the TRAP-L sample was collected 50 cm above the sediment–water interface from summer 2013 to summer 2014. The difference in their sediment composition should thus be mainly influenced by the depth of sedimentation, although 20 mm from the bottom may represent a bit more than a year of sedimentation because of compaction. Considering that the bottom pond waters are poor in oxygen (< 40% DO) during summer, OM is most likely oxidized above and within this zone before reaching the bottom, resulting in the very low LOI of the CORE-S14 sample. Such low OM content in hypoxic bottom waters compared to the oxygen-rich surface was also found in comparable thermokarst ponds south of the BGR site (Bouchard et al., 2014). Aside from the OM proportion, the particle size difference could also be explained by changes in water column parameters, such as differences in salinity and temperature at the pond bottom, which influence density and therefore the settling velocity of particles (Deshpande et al., 2015).

The proportion of OM present in sediments may be partly related to oxidation processes during sedimentation in the water column. OM content decreased with depth, as it was progressively oxidized down the water column during sedimentation, explaining the lower OM content in deeper samples (core samples excluded). DO followed the same decreasing trend with depth, as OM oxidation consumed oxygen. Biochemical degradation of OM could also occur in sediments by anaerobic bacterial activity (Deshpande et al., 2015). The percentages of C, H and N were proportional to OM content and they were all higher in samples from 2013 to 2014 as compared to those from 2012 to 2013.

Although the LOI measurement method used is expected to have up to 2% error within the same sample and that the preprocessing method (freeze drying/oven drying) could slightly affect the LOI results, a relation can be interpreted with other parameters. DO decreases in the BGR1 water column (Fig. 4) and sediment trap LOI follows the same pattern (Table 2). Although the optical trap was tied to the other "simple" traps during 2012–2013, its funnel mouth was 35 cm above those of the other traps (Fig. 3a). TRAP-O yielded a LOI of 11.1%, slightly higher than TRAP-1 and TRAP-2 with 10.4 and 10.4%, respectively. For the period 2013–2014, TRAP-U (2 m depth) and TRAP-L (3 m depth) sediments showed LOI values of 12.5% and 11.9% respectively. The only sediment sample from the bottom center of the pond (CORE-S14), which was poor in oxygen, showed the lowest LOI value (2.3%). The CORE-DEEP sample is likely much older than other samples as it originates from the core, located just above the peat layer (1825–1950 cal yr. BP). Its OM content therefore depends on many factors, including soil properties and geochemical composition at the time of deposition, permafrost extent and depth, the limnological parameters and the sedimentation rate (burial time). Biochemical degradation could have affected this sample since its deposition many centuries ago. The sample could also have been altered by the peat layer just underneath it, which would explain its higher LOI value than that of the CORE-S13 sample, which was at the top of the core. The C, H and N proportions of the samples follow the same trend as the one displayed by LOI values (Table 2). This supports the previous results as these elements usually originate from the organic matter in sediment samples. The percentages of C follow the exact same trend; the H percentages include an exception for the TRAP-O, TRAP-1 and TRAP-2 samples, while the N percentages include an exception for the TRAP-L sample. The Pearson correlation coefficient "r" is >0.99 for LOI/C, LOI/H and LOI/N ratios.

5.4. Sedimentary patterns between the years and possible "life span" of the pond

Based on our two-year sediment traps study, the specific sedimentary patterns can be summarized as follows:

- The sedimentation rate was primarily controlled by meteorological conditions, namely precipitation and temperature. When air temperature was <0 °C, thereby causing ice cover formation on the

pond, the sedimentation rate was nearly zero. Highest sedimentation occurred at the end of summer and during fall, as several months of high temperature led to active layer thawing and the activation of erosional processes (retrogressive slumps and land surface runoff from the catchment). Another high sedimentation period was related to spring runoff directly after ice break-up. In addition, other sedimentation pulses were triggered by either strong precipitation events or prolonged periods during which temperatures remained above 0 °C following snow fall.

- The particle size of samples collected by sediment traps and from the bottom sediments of the pond can be explained by OM content/proportion and the parameters related to the climatic/hydrological conditions of the year of sampling, that is the different strength of runoff, erosion and biological productivity. The plankton constituting most organic matter in the samples could hypothetically be microplankton, as the prevalence of diameters between 30 and 200 μm is correlated to the sample LOI. Particle size also had a coarser main mode in samples from 2012 to 2013 whereas it was finer in samples from 2013 to 2014.
- OM content and C, H, N% of samples were mainly related to the depth of sampling and were higher in samples from 2013 to 2014 as compared to those from 2012 to 2013.

The BGR1 pond is located on impermeable soil (silt-clay), and ground permeability is a determining factor for the hydrological stability of aquatic systems in thermokarst terrain. They usually persist on impermeable soils, whereas they are more likely to become smaller and disappear due to drainage in other regions where soils have a higher hydraulic conductivity (Andresen and Lougheed, 2015). The pond is well isolated from the other ones on the site, so it should not undergo coalescence. If we consider precipitation will be abundant enough to compensate evaporation, the sedimentation rates measured by sediment traps can be used with long-term compaction values for silty sediments and pond depth to approximate the time span needed to completely fill the pond with sediments.

The maximum pond depth measured was 4.3 m in summer 2014. Referring to a model of thermokarst pond development from a lithalsa of the BGR site (Calmels et al., 2008a), the BGR1 pond dimensions suggest that it is close to its maximum depth. Nevertheless, the pond may still be deepening due to surrounding and underlying permafrost thaw, hence the calculated value is a minimum. The optical trap collected nearly 29 mm of sediments between 31 August 2012 and 31 July 2013. Data for the month of August is missing and must be estimated. The end of summer and beginning of fall was the most active part of the year, with the highest monthly sediment accumulation of 10 mm in September. Sediment deposition was likely still not at its highest in August. Therefore, a minimum accumulation of 1 mm and a maximum of 10 mm can be used for this month, yielding a total sediment thickness ranging from 30 to 39 mm for the year.

A long-term compaction coefficient must be used to evaluate the real thickness of sediments undergoing diagenesis once buried. In this situation, sediments can be considered dry, as little water and porosity remain among them. Samples from the bottom of BGR1 (CORE-S13 and CORE-S14) had an average LOI of 2.6%, resulting in a particle density of 2.61 g cm^{-3} (see Section 3.3). Volume calculation requires wet and dry sample weight (from surface sediments). Such data is not available for the samples of this study, but Bouchard et al. (2011) did such calculations on sediments similar to the BGR1 samples from thermokarst ponds near Kuujjuaraapik-Whampagoostui. They contained 30 to 70% silt, 25 to 75% clay and 2.3 to 8.0% LOI, which is very similar to samples of BGR1. Using water content measured in a core between 0 and 3.6 cm depth, the resulting compaction coefficient ranges from 0.240 to 0.298 (Eq. (1)). Using these values, the time required for the infilling ("life span") of the pond BGR1 can be estimated at between 370 and 600 years (Eq. (2)). This is a first approximation with the available data and its accuracy should be further enhanced by taking more factors into consideration. Still, it provides an order of magnitude for the time scale of subarctic thermokarst ponds of small size on impermeable soils in general. It is considerably shorter than the large thermokarst lakes that are the subject of many studies, mainly in Siberia, western Canada and Alaska, which formed many hundreds to thousands of years ago (e.g., Murton, 2001; Morgenstern et al., 2011; Lenz et al., 2013).

6. Conclusions

Sediment samples collected with sediment traps in Nunavik revealed many features of a young thermokarst pond that represents an increasingly common and widespread aquatic system in subarctic regions. The sediment input in the traps was rather high (estimated 30–39 mm/year) and peaked in late summer, as well as at the height of the spring ice and snowmelt period. Variations in sedimentation rates were explained by changes in meteorological conditions, essentially temperature and precipitation. Differences in sedimentation relative to depth were explained by limnological parameters. For example, particle size was influenced by organic matter content, which in turn was associated with DO in the water column and decreased with depth. OM in the sediments was interpreted as mainly autochthonous based on C/N ratios and believed to be composed of microplankton, based on particle size and LOI analysis. However, $\delta^{13}C$ analysis or the microscopic study of smear slides should be conducted to further investigate this hypothesis.

Thermokarst ponds and lakes in the discontinuous permafrost zone have an impact on the landscape, from modifications of permafrost extent and depth to changes of biogeochemical fluxes and dynamics, including the carbon cycle. Thus, it is important to evaluate the "life span" of these widespread systems on impermeable soils such as pond BGR 1. The estimation of its "life span" will refine the time scale of thermokarst pond evolution and help understand its impacts. Our findings further contribute to the development of sediment trap approaches for use in aquatic systems in thermokarst terrain. This two-year study is the first step towards the development of elaborate and accurate models that extend over longer periods of time.

Acknowledgements

Funding was obtained through ADAPT (Arctic Development and Adaptation to Permafrost in Transition) and Natural Sciences and Engineering Research Council of Canada (NSERC-Discovery) grants awarded to RP, and an EnviroNorth scholarship awarded to FB. Logistic support for fieldwork in Nunavik was provided through CEN, the Research Centres of Excellence program ArcticNet and the Northern Scientific Training Program (NSTP). We thank Denis Sarrazin, Valentin Proult, Biljana Narancic, and Olivier Jacques for assistance in the field; Bethany Deshpande and Warwick F. Vincent for providing the water chemistry data; Guillaume Labrecque for laboratory analyses, as well as the people of the hamlets of Whapmagoostui and Kuujjuarapik for hosting the scientific station and equipment for the CEN.

References

Allard, M., Séguin, M.K., 1985. La déglaciation d'une partie du versant hudsonien québécois: bassins des rivières Nastapoca, Sheldrake et à l'Eau Claire. Géographie Physique et Quaternaire 39, 13–24.

Allard, M., Seguin, M.K., 1987. The Holocene evolution of permafrost near the tree line on the eastern coast of Hudson Bay (Northern Quebec). Canadian Journal of Earth Sciences 24, 2206–2222.

Allard, M., Caron, S., Bégin, Y., 1996. Climate and ecological controls on ice segregation and thermokarst: the case study of a permafrost plateau in Northern Québec. Permafrost and Periglacial Processes 7, 207–227.

Andresen, C.G., Lougheed, V.L., 2015. Disappearing Arctic tundra ponds: fine-scale analysis of surface hydrology in drained thaw lake basins over a 65 year period (1948-2013). Journal of Geophysical Research – Biogeosciences 120, 466–479.

Baker, E.T., Milburn, H.B., Tennant, D.A., 1988. Field assessment of sediment trap efficiency under varying flow conditions. Journal of Marine Research 46, 573–592.

Beaulieu, N., Allard, M., 2003. The impact of climate change on an emerging coastline affected by discontinuous permafrost: Manitounuk Strait, Northern Quebec. Canadian Journal of Earth Sciences 40, 1393–1404.
Beck, I., Ludwig, R., Bernier, M., Lévesque, E., Boike, J., 2015. Assessing permafrost degradation and land cover changes (1986-2009) using remote sensing data over Umiujaq, sub-Arctic Québec. Permafrost and Periglacial Processes 26, 129–141.
Bhiry, N., Delwaide, A., Allard, M., Bégin, Y., Filion, L., Lavoie, M., Nozais, C., Payette, S., Pienitz, R., Saulnier-Talbot, É., Vincent, W.F., 2011. Environmental change in the Great Whale River region, Hudson Bay: five decades of multidisciplinary research by Centre d'études nordiques (CEN). Écoscience 18, 182–203.
Bouchard, F., Francus, P., Pienitz, R., Laurion, I., Feyte, S., 2014. Subarctic thermokarst ponds: investigating recent landscape evolution and sediment dynamics in thawed permafrost of northern Québec (Canada). Arctic, Antarctic and Alpine Research 46, 251–271.
Bouchard, F., Francus, P., Pienitz, R., Laurion, I., 2011. Sedimentology and geochemistry of thermokarst ponds in discontinuous permafrost, subarctic Quebec, Canada. Journal of Geophysical Research 116, G00M04. http://dx.doi.org/10.1029/2011JG001675.
Boyd, C.E., 1995. Bottom Soils, Sediment, and Pond Aquaculture. Chapman & Hall, New York (348 pp.).
Buteau, S., Fortier, R., Allard, M., 2010. Permafrost weakening as a potential impact of climate warming. Journal of Cold Regions Engineering 24, 1–18.
Calmels, F., Allard, M., Delisle, G., 2008a. Development and decay of a lithalsa in Northern Québec: A geomorphological history. Geomorphology 97, 287–299.
Calmels, F., Delisle, G., Allard, M., 2008b. Internal structure and the thermal and hydrological regime of a typical lithalsa: significance for permafrost growth and decay. Canadian Journal of Earth Sciences 45, 31–43.
Cayer, D., 2010. Manuel d'analyse granulométrique: méthode combinant les techniques de la granulométrie laser et les tamis. Première éd. Laboratoire de sédimentologie et de géomorphologie, Université Laval (21 pp.).
Chen, M., Rowland, J.C., Wilson, C.J., Altmann, G.L., Brumby, S.P., 2014. Temporal and spatial pattern of thermokarst lake area changes at Yukon flats, Alaska. Hydrological Processes 28, 837–852.
Chouinard, C., Fortier, R., Mareschal, J.C., 2007. Recent climate variations in the subarctic inferred from three borehole temperature profiles in Northern Quebec, Canada. Earth and Planetary Science Letters 263, 355–369.
Czudek, T., Demek, J., 1970. Thermokarst in Siberia and its influence on the development of lowland relief. Quaternary Research 1, 103–120.
Deshpande, B.N., MacIntyre, S., Matveev, A., Vincent, W.F., 2015. Oxygen dynamics in permafrost thaw lakes: anaerobic bioreactors in the Canadian subarctic. Limnology and Oceanography 60, 1656–1670.
Dyke, A.S., Prest, V.K., 1987. Late Wisconsinan and Holocene history of the laurentide ice sheet. Géographie Physique et Quaternaire 41, 237–263.
Environment Canada, 2015. 1981–2010 Climate normals & average. http://climate.weather.gc.ca/climate_normals/index_e.html (Last accessed 2015–06-22).
Fortier, R., LeBlanc, A.M., Allard, M., Buteau, S., Calmels, F., 2008. Internal structure and conditions of permafrost mounds at Umiujaq in Nunavik, Canada, inferred from field investigation and electrical resistivity tomography. Canadian Journal of Earth Sciences 45, 367–387.
Gardner, W.D., 1977. Fluxes, dynamics and chemistry of particulates in the ocean (Unpublished Ph.D. Thesis) MIT/WHOI Joint Program in Oceanography (405 pp.).
Gardner, W.D., 1980a. Field assessment of sediment traps. Journal of Marine Research 38, 41–52.
Gardner, W.D., 1980b. Sediment trap dynamics and calibration: a laboratory evaluation. Journal of Marine Research 38, 17–39.
Hargrave, B.T., Burns, N.M., 1979. Assessment of sediment trap collection efficiency. Limnology and Oceanography 24, 1124–1136.
Heiri, O., Lotter, A.F., Lemcke, G., 2001. Loss on ignition as a method for estimating organic and carbonate content in sediments: reproducibility and comparability of results. Journal of Paleolimnology 25, 101–110.
Hillaire-Marcel, C., 1976. La déglaciation et le relèvement isostatique sur la côte est de la baie d'Hudson. Cahiers de Géographie de Québec 20, 185–220.
Hillaire-Marcel, C., Fairbridge, R.W., 1978. Isostasy and eustasy of Hudson Bay. Geology 6, 117–122.
Honjo, S., Doherty, K.W., 1988. Large aperture time-series sediment traps; design objectives, construction and application. Deep-Sea Research 35, 133–149.
Hugelius, G., Strauss, J., Zubrzycki, S., Harden, J.W., Schuur, E.A.G., Ping, C.L., Schirrmeister, L., Grosse, G., Michaelson, G.J., Koven, C.D., O'Donnell, J.A., Elberling, B., Mishra, U., Camill, P., Yu, Z., Palmtag, J., Kuhry, P., 2014. Estimated stocks of circumpolar permafrost carbon with quantified uncertainty ranges and identified data gaps. Biogeosciences 11, 6573–6593.
Iwahana, G., Fukui, K., Mikhailov, N., Ostanin, O., Fuji, Y., 2012. Internal structure of a lithalsa in the Akkol Valley, Russian Altai Mountains. Permafrost and Periglacial Processes 23, 107–118.
Jolivel, M., Allard, M., 2013. Thermokarst and export of sediment and organic carbon in the Sheldrake River watershed, Nunavik, Canada. Journal of Geophysical Research: Earth Surface 118, 1729–1745.
Jones, B.M., Arp, C.D., 2015. Observing a catastrophic thermokarst Lake Drainage in Northern Alaska. Permafrost and Periglacial Processes 26, 119–128.
Jones, B.M., Grosse, G., Arp, C.D., Jones, M.C., Walter Anthony, K.M., Romanovsky, V.E., 2011. Modern thermokarst lake dynamics in the continuous permafrost zone, northern Seward Peninsula, Alaska. Journal of Geophysical Research 116, G00M03. http://dx.doi.org/10.1029/2011JG001666.
Kirchner, W.B., 1975. An evaluation of sediment trap methodology. Limnology and Oceanography 20, 657–660.
Köster, D., Pienitz, R., 2006. Seasonal diatom variability and paleolimnological inferences – a case study. Journal of Paleolimnology 35, 395–416.
Lamarre, A., Garneau, M., Asnong, H., 2012. Holocene paleohydrological reconstruction and carbon accumulation of a permafrost peatland using testate amoeba and macrofossil analyses, Kuujjuarapik, subarctic Québec, Canada. Review of Palaeobotany and Palynology 186, 131–141.
Lamoureux, S.F., 2005. A sediment accumulation sensor for use in lacustrine and marine sedimentation studies. Geomorphology 68, 17–23.
Laurion, I., Vincent, W.F., MacIntyre, S., Retamal, L., Dupont, C., Francus, P., Pienitz, R., 2010. Variability in greenhouse gas emissions from permafrost thaw ponds. Limnology and Oceanography 55, 115–133.
Lavoie, C., Allard, M., Duhamel, D., 2012. Deglaciation landforms and C-14 chronology of the Lac Guillaume-Delisle area, eastern Hudson Bay: A report on field evidence. Geomorphology 159-160, 142–155.
Lenz, J., Fritz, M., Schirrmeister, L., Lantuit, H., Wooller, M.J., Pollard, W.H., Wetterich, S., 2013. Periglacial landscape dynamics in the western Canadian Arctic: results from a thermokarst lake record on a push moraine (Herschel island, Yukon territory). Palaeogeography, Palaeoclimatology, Palaeoecology 381-382, 15–25.
Meyers, P.A., Teranes, J.L., 2001. Sediment organic matter. In: Last, W.M., Smol, J.P. (Eds.), Tracking Environmental Changes Using Lake Sediments—Volume II: Physical and Chemical Techniques. Kluwer, Dordrecht, pp. 239–269.
Morgenstern, A., Grosse, G., Günther, F., Fedorova, I., Schirrmeister, L., 2011. Spatial analyses of thermokarst lakes and basins in yedoma landscapes of the Lena Delta. The Cryosphere 5, 849–867.
Murton, J.B., 2001. Thermokarst sediments and sedimentary structures, Tuktoyaktuk coastlands, western Arctic Canada. Global and Planetary Change 28, 175–192.
Phelps, A.R., Peterson, K.M., Jeffries, M.O., 1998. Methane efflux from high-latitude lakes during spring ice melt. Journal of Geophysical Research 103, 29029–29036.
Proult, V., 2014. Lorigine périglaciaire et son influence sur les écosytèmes thermokarstiques au Nunavik: Analyse des communautés d'algues silicieuses (Unpublished M. Sc. Thesis) Université Laval (225 pp.).
Romanovsky, V.E., Drozdov, D.S., Oberman, N.G., Malkova, G.V., Kholodov, A.L., Marchenko, S.S., Moskalenko, N.G., Sergeev, D.O., Ukraintseva, N.G., Abramov, A.A., Gilichinsky, D.A., Vasiliev, A.A., 2010b. Thermal state of permafrost in Russia. Permafrost and Periglacial Processes 21, 136–155.
Romanovsky, V.E., Smith, S.L., Christiansen, H.H., 2010a. Permafrost thermal state in the polar Northern Hemisphere during the International Polar Year 2007-2009: a synthesis. Permafrost and Periglacial Processes 21, 106–116.
Schuur, E.A.G., Bockheim, J.G., Canadell, J.G., Euskirchen, E., Field, C.B., Goryachkin, S.V., Hagemann, S., Kuhry, P., Lafleur, P.M., Lee, H., Mazhitova, G., Nelson, F.E., Rinke, A., Romanovsky, V.E., Shiklomanov, N., Tarnocai, C., Venevsky, S., Vogel, J.G., Zimov, S.A., 2008. Vulnerability of permafrost carbon to climate change: implications for the global carbon cycle. Bioscience 58, 701–714.
Schuur, E.A.G., Vogel, J.G., Crummer, K.G., Lee, H., Sickman, J.O., Osterkamp, T.E., 2009. The effect of permafrost thaw on old carbon release and net carbon exchange from tundra. Nature 459, 556–559.
Smith, L.C., Sheng, Y., MacDonald, G.M., Hinzman, L.D., 2005. Disappearing Arctic Lakes. Science 308, 1429-1429.
Smith, S.L., Romanovsky, V.E., Lewkowicz, A.G., Burn, C.R., Allard, M., Clow, G.D., Yoshikawa, K., Throop, J., 2010. Thermal state of permafrost in North America: A contribution to the International Polar Year. Permafrost and Periglacial Processes 21, 117–135.
Smith, S.L., Throop, J., Lewkowicz, A.G., 2012. Recent changes in climate and permafrost temperatures at forested and polar desert sites in Northern Canada. Canadian Journal of Earth Sciences 49, 914–924.
Stuiver, M., Reimer, P.J., Reimer, R.W., 2005. CALIB 5.0. [WWW program and documentation]. http://calib.qub.ac.uk.
Thériault, R., Beauséjour, S., 2012. Geological Map of Quebec [electronic resource]. Géologie Québec, Québec 9782550662204.
Thibault, S., Payette, S., 2009. Recent permafrost degradation in bogs of the James Bay area, Northern Quebec, Canada. Permafrost and Periglacial Processes 20, 383–389.
Vallée, S., Payette, S., 2007. Collapse of permafrost mounds along a subarctic river over the last 100 years (northern Québec). Geomorphology 90, 162–170.
Walter Anthony, K.M., Zimov, S.A., Grosse, G., Jones, M.C., Anthony, P.M., Chapin III, F.S., Finlay, J.C., Mack, M.C., Davydov, S., Frenzel, P., Frolking, S., 2014. A shift of thermokarst lakes from carbon sources to sinks during the Holocene epoch. Nature 511, 452–456.
Walter, K.M., Zimov, S.A., Chanton, J.P., Verbyla, D., Chapin, F.S.I.I.I., 2006. Methane bubbling from Siberian thaw lakes as positive feedback to climate warming. Nature 443, 71–75.
Yi, S., Wischnewski, K., Langer, M., Muster, S., Boike, J., 2014. Freeze/thaw processes in complex permafrost landscapes of northern Siberia simulated using the TEM ecosystem model: impact of thermokarst ponds and lakes. Geoscientific Model Development 7, 1671–1689.